

IMU Preintegrated Features for Efficient Deep Inertial Odometry

Rooholla Khorrambakht

K.N.Toosi University of Technology
Tehran, Iran
r.khorrambakht@email.kntu.ac.ir

Hamed Damirchi

K.N.Toosi University of Technology
Tehran, Iran
hdamirchi@email.kntu.ac.ir

Hamid D. Taghirad

K.N.Toosi University of Technology
Tehran, Iran
taghirad@kntu.ac.ir

ABSTRACT

MEMS Inertial Measurement Units (IMUs) as ubiquitous proprioceptive motion measurement devices are available on various everyday gadgets and robotic platforms. Nevertheless, the direct inference of geometrical transformations or odometry based on these data alone is a challenging task. This is due to the hard-to-model imperfections and high noise characteristics of the sensor, which has motivated research in formulating the system as an end-to-end learning problem, where the motion patterns of the agent are exploited to facilitate better odometry estimates. However, this benefit comes at the cost of high computation and memory requirements, which makes deep inertial odometry unsuitable for low-power and edge applications. This paper attempts to address this conflict by proposing the IMU preintegrated features as a replacement for the raw IMU data in deep inertial odometry. Exploiting the manifold structure of the IMU motion model, these features provide a temporally compressed motion representation that preserves important geometrical information. We demonstrate the effectiveness and efficiency of this approach for the task of inertial odometry on two applications of pedestrian motion estimation and autonomous vehicles. We show a performance improvement compared to raw inputs while reducing the computational burdens. Additionally, we demonstrate the efficiency of this approach through an embedded implementation on a resource-constrained microcontroller.

KEYWORDS

IMU preintegration, deep inertial odometry, autonomous vehicles, pedestrian tracking

ACM Reference Format:

Rooholla Khorrambakht, Hamed Damirchi, and Hamid D. Taghirad. 2022. IMU Preintegrated Features for Efficient Deep Inertial Odometry. In *Proceedings of tinyML Research Symposium (tinyML Research Symposium '22)*. ACM, New York, NY, USA, 6 pages.

1 INTRODUCTION

With the advent of MEMS Inertial Measurement Units (IMUs) as low-power and low-cost proprioceptive motion sensors, this modality has been added to numerous everyday gadgets and autonomous systems. Smartphones and smartwatches, autonomous vehicles, VR¹ headsets, and even gaming consoles all contain some variant

¹Virtual Reality

Permission to make digital or hard copies of part or all of this work for personal or classroom use is granted without fee provided that copies are not made or distributed for profit or commercial advantage and that copies bear this notice and the full citation on the first page. Copyrights for third-party components of this work must be honored. For all other uses, contact the owner/author(s).

tinyML Research Symposium '22, March 2022, San Jose, CA
© 2022 Copyright held by the owner/author(s).

of this sensor. This widespread availability of this modality has encouraged new applications such as user activity recognition [10] and pedestrian tracking [9] for situations where other sensors may fail.

However, the expense of their lower cost and smaller form factor, is that MEMS IMUs are much more challenging to model accurately due to the manufacturing imperfections, high and time-variant noise characteristics, and nonlinear effects. While many prominent classical pipelines based on statistical sensor fusion and optimization systems already exist for the efficient incorporation of IMUs into various applications [14, 16], there are many scenarios where the restricting assumptions of the system's formulation limit the application and robustness of the method.

These challenges have encouraged researchers to consider deep learning methods to enable previously implausible applications of this modality as independent sensors. The ability to learn high-dimensional latent presentations from data enables these methods to exploit the underlying motion patterns of the agent to reduce the odometry drift.

Generally, there are two lines of research in this field. Many works try to exploit leaned models as modules within a classical fusion system to detect important motion events. For instance, [18] proposes using an LSTM to detect zero-velocity events in human walking to reset the states of an Extended Kalman Filter (EKF) and avoid the accumulation of error. In a similar attempt, [4] designs a classifier that detects specific motion modes of a wheeled vehicle and uses the classifier's results to define a set of pseudo measurements for an Invariant Extended Kalman Filter.

On the other hand, the opposing approach is to cast the problem as a pure data-driven pipeline and synthesize models that directly consume raw sensor data to yield the final prediction. For instance, [5] proposes using an LSTM model for predicting the human trajectory represented in polar coordinates. Furthermore, this end-to-end application of IMUs has also been considered alongside other modalities such as vision [2, 6], and thermal images [17] to estimate the ego-motion of a robot or autonomous vehicle.

While the former approaches are computationally efficient due to their classical core and minimal models, they are highly limited to the design domain for which they are engineered. On the other hand, even though the data-driven methods are highly flexible and general, they lack the computational efficiency of their classical counterparts, and they may not be easily used for low-power embedded and wearable applications.

This paper aims to address this conflict by proposing an efficient and temporally compact motion representation that draws inspiration from the preintegration theory known to the graph-based Visual-Inertial Odometry (VIO) community [12]. While [12] formulates the preintegration as part of a classical VIO optimization problem and as a motion constraint, the novelty of this approach is in the

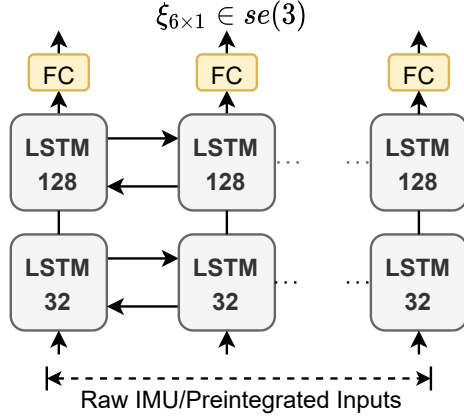


Figure 1: The baseline model for investigating the effectiveness of preintegrated features.

repurposing of this geometrical constraint as a preprocessing/input-feature for learning-based models. This input feature replaces the raw IMU data and in doing so, improves the performance while extensively reducing the computational burdens. Finally, the efficiency of this approach has been further illustrated by providing an embedded implementation of a deep pedestrian inertial odometry pipeline on a microcontroller with highly restricted resources.

The rest of this paper is organized as follows. Section 2 introduces the Preintegrated features and describes the baseline models and the training procedure used to demonstrate the effectiveness of the proposed approach. Then, Section 3 presents the experimental setups and the results of applying preintegration for the two tasks of pedestrian and autonomous vehicles inertial odometry. Furthermore, this section also demonstrates the computational efficiency of the approach through the embedded implementation of IO-Net [9] with preintegrated IMU inputs, and finally, Section 4 concludes the paper and proposes future directions.

2 METHODOLOGY

This section introduces the methodology for extraction of preintegrated features from IMU raw data and presents the baseline architecture and training procedure used to demonstrate their application in deep inertial odometry.

2.1 IMU Preintegrated Features

Preintegrated IMU features draw inspiration from the factor graph approach to Visual Inertial Odometry (VIO) [12]. Factor graphs are Probabilistic Graphical Models (PGM) that provide a natural language to describe many optimization problems in robotics and SLAM² [11]. In this formulation, the IMU constrains the motion in between keyframes based on linearization-point independent energy factors formulated using the kinematic measurement model

of an IMU [12]:

$$\begin{aligned} \mathbf{R}_{n+1} &= \mathbf{R}_n \exp((\tilde{\omega}_n - \mathbf{b}_g - \boldsymbol{\eta}_g)^\wedge \Delta t) \\ \mathbf{v}_{n+1} &= \mathbf{v}_n + \mathbf{g}\Delta t + \mathbf{R}_n(\tilde{\mathbf{a}}_n - \mathbf{b}_a - \boldsymbol{\eta}_a) \\ \mathbf{p}_{n+1} &= \mathbf{p}_n + \mathbf{v}_n\Delta t + \frac{1}{2}\mathbf{g}\Delta t^2 + \mathbf{R}_n(\tilde{\mathbf{a}}_n - \mathbf{b}_a - \boldsymbol{\eta}_a)\Delta t^2 \end{aligned} \quad (1)$$

where \mathbf{R}_n , \mathbf{v}_n , and \mathbf{p}_n are orientation, velocity and position of the sensor with respect to the world frame, and Δt is the sampling time of the IMU. The angular velocity and acceleration measurements $\tilde{\omega}_n$, $\tilde{\mathbf{a}}_n$ from the gyroscope and accelerator are contaminated with additive Gaussian noise $\boldsymbol{\eta}_g$, $\boldsymbol{\eta}_a$ and random walk bias terms \mathbf{b}_g , \mathbf{b}_a . Furthermore, the $\exp(\cdot)$ is the SO3 exponential map that links lie algebra $\mathfrak{so}(3)$ vectors to their corresponding SO3 matrices.

Batches of IMU measurements between two i and j keyframes may be compressed into motion constraints by integrating the above equations. Nevertheless, the outcome of this integration changes with the initial condition at time i . Multiplying both sides of this integration by \mathbf{R}_i breaks this dependence and yields the following initial conditions independent constraints [12]:

$$\begin{aligned} \Delta \mathbf{R}_{ij} &\triangleq \mathbf{R}_i^\top \mathbf{R}_j = \prod_{k=i}^{j-1} \exp\left(\left(\tilde{\omega}_k - \mathbf{b}_k^g - \boldsymbol{\eta}_k^g\right) \Delta t\right) \\ \Delta \mathbf{v}_{ij} &\triangleq \mathbf{R}_i^\top \left(\mathbf{v}_j - \mathbf{v}_i - \mathbf{g}\Delta t_{ij}\right) \\ &= \sum_{k=i}^{j-1} \Delta \mathbf{R}_{ik} \left(\tilde{\mathbf{a}}_k - \mathbf{b}_k^a - \boldsymbol{\eta}_k^a\right) \Delta t \\ \Delta \mathbf{p}_{ij} &\triangleq \mathbf{R}_i^\top \left(\mathbf{p}_j - \mathbf{p}_i - \mathbf{v}_i\Delta t_{ij} - \frac{1}{2} \sum_{k=i}^{j-1} \mathbf{g}\Delta t^2\right) \\ &= \sum_{k=i}^{j-1} \left[\Delta \mathbf{v}_{ik}\Delta t + \frac{1}{2} \Delta \mathbf{R}_{ik} \left(\tilde{\mathbf{a}}_k - \mathbf{b}_k^a - \boldsymbol{\eta}_k^a\right) \Delta t^2\right] \end{aligned} \quad (2)$$

In this paper, we exploit these on-manifold integrated motion constraints as efficient motion features for learning-based models. In other words, rather than feeding a recurrent neural network (RNN) with the raw and high-frequency IMU data, we use preintegration in order to reduce the temporal dimension of the inputs, which is the root of the achieved efficiency. Moreover, the reduced temporality and the induced geometrical bias in formulating this input leads to improved predictive performance as shown in our experiments.

It is important to note that in this work, we disregard the biases in Eq. 2 by assigning them with random values during the training as a data augmentation technique.

2.2 The Baseline Model

2.2.1 The Network Architecture. Drawing inspiration from the double integration nature of the IMU kinematics model, we have adopted a two-layer bidirectional LSTM architecture as our baseline neural network. As illustrated in Fig. 1, this model is comprised of two layers with 32 and 128 hidden units. The features extracted by the second LSTM layer are then linearly mapped into 6-DOF $\mathfrak{se}(3)$ odometry labels. These $\mathfrak{se}(3)$ vectors are the logarithmic maps of the expected $SE(3)$ odometry transformations between poses T_{i-1} and T_i :

²Simultaneous Localization and Mapping

$$\xi_i = \log(T_{i-1}^{-1}T_i)^\vee \in \mathbb{R}^6 \quad (3)$$

Our motivation for bi-directionality is the ability of this model to attend to both future and the past samples within a window of IMU measurements, and we have chosen the larger 128-unit hidden size for the second layer to facilitate better $\mathfrak{se}(3)$ regression. Overall, the baseline model has 210K parameters.

2.2.2 Loss Formulation. We adopt the formulation presented in [15] and formulate the training loss as the weighted sum of squares of the geodesic distances between the ground truth odometry labels, $\Delta T^*_{i-1,i} = T^*_{i-1}^{-1}T^*_i$, and the network’s outputs as follows:

$$L = \sum_{k=1}^N g_i^T \Sigma^{-1} g_i \quad (4)$$

$$g_i = \log(\Delta T^*_{i,i+1} \exp(\xi_i^\wedge))^\vee$$

Where $(\cdot)^\wedge$ and $(\cdot)^\vee$ operators respectively transform the $\mathfrak{se}(3)$ vectors into their skew symmetric matrix form and vice versa. The Σ parameter in the above equation is an empirical covariance matrix computed using the training data based on the following equations:

$$\Sigma = \frac{1}{N-1} \sum_{i=1}^N (\xi_i^* - \bar{\xi}^*) (\xi_i^* - \bar{\xi}^*)^T \quad (5)$$

$$\bar{\xi}^* \triangleq \frac{1}{N} \sum_{i=1}^N \xi_i^*$$

where N is the number of labels in the training dataset, and $\xi_i^* = \log(\Delta T_{i-1,i})^\vee$. The computed covariance in the above equation balances the relative importance of each motion axis and stabilizes the training.

3 EXPERIMENTS AND STUDIES

3.1 Datasets

We evaluate our approach on two different application domains: (1) autonomous driving, and (2) pedestrian odometry. For *autonomous driving*, the KITTI odometry dataset [13] has been chosen. This dataset is recorded using a car equipped with vision, Lidar, and RTK-GPS+IMU units traveling around urban and countryside environments. The IMU data is recorded at a rate of 100 Hz, and the ground truth is provided at 10 Hz through a batch maximum likelihood estimation based on Lidar and GPS data.

For the *pedestrian odometry* application, the handheld and trolley domains of the OxfordIO dataset [8] have been chosen. OxfordIO dataset contains the IMU readings from a smartphone held in various configurations and carried by a user while undergoing different motion patterns. The ground truth for this dataset is provided using a Vicon motion capture system with millimeter-level accuracy.

3.2 Baseline Implementation

We implemented our model using PyTorch and PytorchLightning frameworks and ran the training process on an Nvidia T4 GPU. Adam optimizer with a learning rate of 0.001 is used to train the models. On average, the convergence happened after 120 epochs. To avoid overfitting, dropout layers have been used after each LSTM

Table 1: Relative odometry translation (%) and orientation (deg/100m) errors on the KITTI dataset.

test seq.	Raw IMU		Averaged IMU		PI-Features (ours)	
	t_{rel}	r_{rel}	t_{rel}	r_{rel}	t_{rel}	r_{rel}
05	10.95	2.06	17.02	2.73	4.75	0.85
07	16.07	4.42	14.04	2.04	9.06	1.56
10	7.57	1.52	9.03	2.41	5.26	0.75
avg.	11.53	2.66	13.36	2.38	6.35	1.05

layer to zero out 25% of the neuron activities at each iteration. Our implementations will be open sourced³.

3.3 Baseline Results

3.3.1 Autonomous Driving. In this section we train three models. As the base of comparison, we train our baseline model using raw IMU data over 1280 IMU samples which corresponds to 12.8 seconds of IMU measurements. Furthermore, to compare preintegration with a naive Euclidean averaging, we averaged each 10 IMU sample into one measurement and trained a model with 128 such measurements. Finally, our main experiment trains the baseline model on preintegrated features each computed over 10 IMU samples, which leads to 128 input features. Our motivation for choosing an integration factor of 10 has been the 10 Hz ground-truth frequency of the KITTI dataset as opposed to the 100 Hz IMU samples.

The test/train splitting policy for the KITTI dataset follows the common practice in data-driven VIO literature [7], which takes sequences 05, 07, and 10 for testing, and sequences {00-10}-{05,07,10,03} for training. We report our results as relative translation and rotation errors defined by the KITTI benchmark [13]. These relative errors are defined as the averaged position/orientation errors within all possible sub-sequences of lengths 100m, ..., 800m.

Table 1 represents the overall comparison between the results of our three experiments. As it can be seen from the first and second columns of the table, the average translation and orientation errors of averaged measurements is the lowest and as shown in the third column, the baseline model trained using the preintegrated features consistently achieves the best results compared to both averaged and raw inputs. This performance improvement is also qualitatively evident from Fig. 2. As shown in this figure, the models trained using the preintegrated IMU features exhibit better orientation stability which in turn leads to better translational accuracy.

We believe that the geometrical inductive bias in calculating the preintegrated features and the reduced burden of memorizing long sequences of raw measurements contribute to this performance improvement when using preintegrated features. Furthermore, as shown in the second column of the table, a naive averaging of the IMU measurements leads to information loss and loss of performance compared to a model trained using raw IMU inputs.

3.3.2 Pedestrian Odometry. We also investigate the effectiveness of our approach for the domain of pedestrian odometry using the OxfordIO dataset. Since naive averaging was shown to be ineffective for deep inertial odometry in the previous section, this section

³https://github.com/Rooholla-KhorramBakht/pi_net

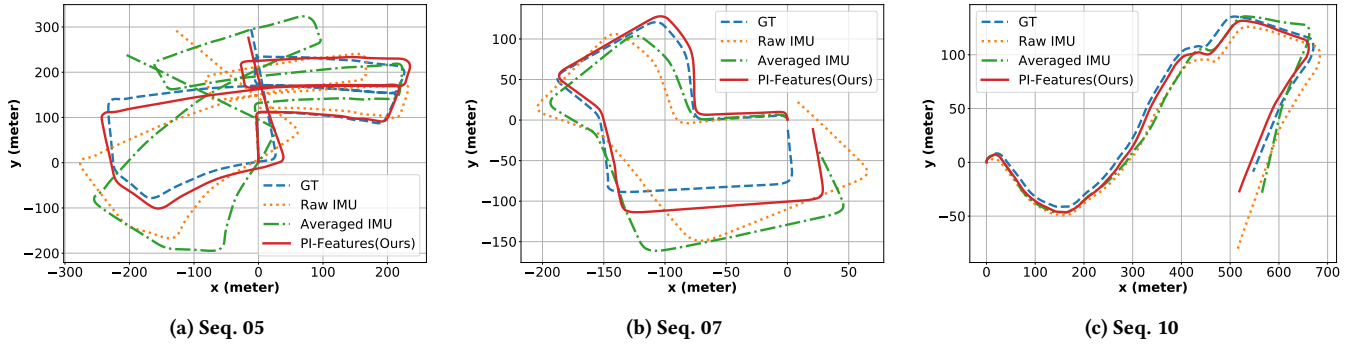


Figure 2: Qualitative comparison between the baseline model with raw, averaged, and preintegrated IMU inputs on KITTI datasets. This figure is best viewed in the color version.

Table 2: Relative translation errors on OxfordIO dataset (handheld/trolley-data#-sequence#)

Method	h-d1-s2	h-d1-s5	h-d1-s6	h-d3-s1	h-d4-s1	h-d4-s3	h-d5-s1	t_d2_s6	average
PI Features (Ours) (%)	5.52	2.66	2.98	3.64	4.16	3.27	3.3	7.61	4.14
Raw IMU (%)	6.5	3.33	3.12	4.45	4.32	4.6	3.64	4.87	4.35

considers only the model trained using the raw IMU inputs as the baseline.

As a metric, we integrate the 6-DoF odometry outputs from both models for batches of 200 IMU measurements, which translates to 2 seconds of walking. The two predictions are then compared against the ground truth to compute the error for each model. We then divide these errors by the displacement length to normalize them.

The experiments in the OxfordIO dataset have been carried out for the trolley and handheld motion domains. The relative translation errors are described in Table 2. As it can be seen from comparing errors in the first and second row of Table 2, a model trained with preintegrated IMU features as input consistently surpasses the baseline trained using the raw IMU measurements.

The only exception is for the trolley domain. Our intuition is that the model trained using the raw data on the trolley domain enjoys the unattenuated high-frequency contents induced by the vibrations of the wheel. This spectral modality helps the model to distinguish various motion states of the trolley and is filtered out by the low pass nature of the integration in the computation of the preintegrated features. As a future research direction, we aim to investigate the extension of preintegrated features with spectral information.

3.4 Embedded Implementation

The baseline architectures in the previous subsection were executed on an NVIDIA GTX1050 GPU and required 1ms to process 20 × 9 PI features and 3.7ms for its corresponding 200 × 6 raw IMU samples (two seconds of data in our datasets). This substantial performance improvement is due to the compressed temporal dimension of the IMU thus fewer LSTM recursions. In this section, we aim to show that IMU preintegration can enable deep inertial odometry even for highly constrained platforms such as microcontrollers. To this aim, we reproduce the IO-Net formulation of deep inertial odometry [9]. Specifically, we train a small Convolutional Neural Network

(CNN) that takes a 2D 9 × T feature map created by stacking T preintegrated IMU features as input and predicts the corresponding translation and heading change in polar coordinate. For comparison purposes, we also construct a bi-LSTM model with the same output format. Two versions of this baseline are then trained using the preintegrated features and raw IMU measurements as inputs.

3.4.1 Architecture. The architecture of the LSTM baseline is similar to the model shown in Fig. 1. The only difference is that the predictions are taken from the feature map of the last timestamp, and the number of hidden units are chosen to be 128 and 256 for the first and second layers to match the values reported in [9]. The feature map corresponding to the last timestamp is then linearly mapped to a ΔΦ and ΔL polar odometry prediction. Similar to the design choice of the IO-Net implementation, we break the raw IMU data into separate windows of 200 samples (2 seconds) and process each of them individually to yield the odometry output (ΔL, ΔΦ) in polar coordinates. Each odometry output updates the subject’s position based on the following kinematic model:

$$\begin{cases} \Phi_{n+1} &= \Phi_n + \Delta\Phi \\ X_n &= X_{n-1} + \Delta L \cos(\Phi_n) \\ Y_n &= Y_{n-1} + \Delta L \sin(\Phi_n) \end{cases} \quad (6)$$

Based on the above equation, the old heading Φ_n is updated using the ΔΦ odometry output. The updated Φ_{n+1} is then used alongside the odometry output ΔL to update the position P_n = [X_n, Y_n]^T.

A smaller feedforward CNN model has been chosen for the microcontroller implementation. As shown in Fig. 3, this model takes the stacked PI features as input and passes them through two CNN layers, one with a kernel size of 3 × 3 × 16 and the other with a kernel size of 1 × 1 × 4. The extracted feature is eventually mapped into two scalar outputs corresponding to the ΔΦ and ΔL polar odometry predictions.

It is important to note that the temporally compressed preintegrated features enable shallow CNNs to cover a much larger temporal receptive field of the motion signal. As a result, one may drastically shrink the model dimension and kernel sizes which facilitate the embedded implementation of the model.

3.4.2 Training and Metrics. We train the model using the mean squared difference between the expected and predicted polar values which is formulated as follows:

$$L = \sum_{i=1}^N \|\Delta L_i - \hat{\Delta L}_i\|_2^2 + \beta \|\Delta \Phi_i - \hat{\Delta \Phi}_i\|_2^2 \quad (7)$$

where N is the number of training sequences in the batch, $\Delta L_i, \Delta \Phi_i$ are the network's outputs, and $\hat{\Delta L}_i, \hat{\Delta \Phi}_i$ are the ground-truth labels. Furthermore, the β hyperparameter in the above equation provides a balance between the orientation and translation components of the loss. This paper sets this parameter based on the average norm of the orientation and translation losses on a randomly initialized model such that the two terms would contribute equally in the backpropagation.

$\Delta \hat{\Phi}_i$ heading label is the projection of the orientation difference between the first and the last sample in the window, and is calculated as follows:

$$\Delta \hat{\Phi}_i = \log(\mathbf{R}_i^T \mathbf{R}_{i+199})^\vee \quad (8)$$

where $\log(\cdot)$ function in the above equation is the $SO3$ logarithmic map and R_i represents the ground-truth label for the i^{th} sample. Furthermore, $\hat{\Delta L}_i$ is calculated as the Euclidean distance between the x-y projections of the first and the last position within a window:

$$\hat{\Delta L}_i = \sqrt{(X_i - X_{i+199})^2 + (Y_i - Y_{i+199})^2} \quad (9)$$

The Root Mean Square Error (RMSE) metric has also been adopted for comparing the results quantitatively. Instead of comparing the integrated paths, we opt to compare the odometry outputs since it provides a more direct comparison.

3.4.3 Performance of The Trained Models. Table 3 presents the model's performances on slow walking, running, phone in pocket, and phone in the handbag domains. The reported numbers are the average rate of change for the heading and stride predictions, $(\Delta L/\Delta T, \Delta \Phi/\Delta T)$. The first and the second columns present the baseline LSTM model trained using the raw inputs, and the second column represents the result trained using the preintegrated features.

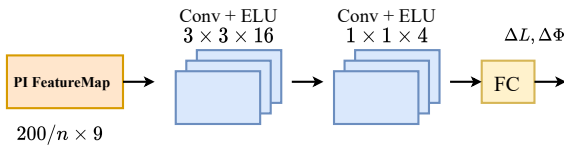


Figure 3: The proposed CNN model for the embedded implementation of the IO-Net pedestrian odometry. In the figure, n is the integration length and in this paper is set to 10.

Furthermore, The third column presents the performance of the small CNN model. As verified in the previous sections, with preintegration, the heading and stride predictive performance is improved compared to the model trained with raw inputs. On the other hand, we can see that the CNN model performs reasonably well even though its complexity is highly reduced compared to the stacked LSTM baseline. Despite this simplicity, it is interesting to note that the CNN model trained on preintegrated inputs performs on par with the baseline IO-Net trained using raw measurements.

3.4.4 Implementation. The embedded implementation of the CNN model is carried out using the X-Cube-AI framework [1], and the preintegration processing has been implemented using the highly optimized ARM CMSIS-DSP math library. While we could have quantized the Keras model for improving its performance, we used the floating-point version due to its generality and faster implementation. On the lowest level of the X-Cube-AI framework, a run-time utilizes the ARM CMSIS-NN/DSP libraries [3] to run the converted Keras network efficiently. The user application may then load the run-time with the appropriate network for inference. In this paper, the target platform is an ARM STM32F407ZET microcontroller with 198KB of RAM and 512KB of flash memory, and with a Cortex-M4 CPU running at 168Mhz. Table 4 presents the implementational details of the CNN model on this microcontroller. As seen in the table, calculating each preintegration vector takes about 0.2ms while each model inference requires only 5ms of computational time. Assuming a stride of 10 (running the inference after each 10 IMU measurements), each inference requires calculating one preintegrated feature and running one model inference, which in total takes 5.2ms. Since this computation is required every 100 milliseconds, there will be plenty of CPU time left for other user-specific tasks.

Furthermore, the model's memory consumption is reasonably low and is around 92.55/512KB for flash and 12.28/192KB for RAM which leaves plenty of room for other user-specific data and code. Furthermore, the successful processing of the preintegration vectors in the microcontroller required increasing the stack to 4KB which is reported here as the approximate required RAM for performing preintegration.

4 CONCLUSIONS AND FUTURE WORKS

This paper proposed a computationally efficient preprocessing method for raw IMU measurements that utilizes the manifold structure of the IMU model to compress long sequences of raw measurements into short and effective motion representations for deep inertial odometry. This compression improves the computational efficiency of deep motion estimation in embedded applications. In addition to this added efficiency, this paper showed improved odometry performance based on preintegrated features through experiments carried out in two distinct domains of pedestrian inertial odometry and autonomous vehicles. Finally, the efficiency of our approach was demonstrated through the formulation of a well-known pedestrian odometry model based on preintegrated features and its implementation on an embedded microcontroller with highly-restricted resources. Prominent directions for future research are applying preintegration for other applications such

Table 3: RMS error of CNN and baseline IO-Net models trained using preintegrated and raw IMU measurements.

	Base Model ($\Delta L(m/S), \Delta\Phi(rad/S)$)	Model with Preintegrated Input ($\Delta L(m/S), \Delta\Phi(rad/S)$)	Embedded CNN Model ($\Delta L(m/S), \Delta\Phi(rad/S)$)
Slow Walking	(0.18, 0.013)	(0.017, 0.013)	(0.029, 0.013)
Running	(0.125, 0.255)	(0.1, 0.216)	(0.115, 0.26)
Pocket	(0.0141, 0.025)	(0.014, 0.025)	(0.021, 0.027)
Handbag	(0.041, 0.0261)	(0.032, 0.081)	(0.048, 0.081)

Table 4: Resource consumption and performance on an STM32F407ZET microcontroller with 512KBi of Flash and 192KBi of RAM running at a clock frequency of 168MHz.

Process	RAM Usage (KB)	ROM Usage (KB)	Execution Time (ms)
Preintegration (per vector)	4 (Stack Size)	0 (No Parameters)	0.2
Model Inference	12.28	92.55	5

as human activity recognition and visual-inertial odometry. Furthermore, the proposed PI feature may be enriched using acoustic features such as FFTs to encode the vibration modality alongside the preintegrated motion vectors, which may provide further improvements in terms of accuracy and robustness.

REFERENCES

[1] 2020. *Getting started with X-CUBE-AI Expansion Package for Artificial Intelligence (AI) UM2526 User manual*. Technical Report.

[2] Yasin Almalioglu, Mehmet Turan, Alp Eren Sari, Muhamad Risqi U. Saputra, Pedro P. B. de Gusmão, Andrew Markham, and Niki Trigoni. 2019. SelfVIO: Self-Supervised Deep Monocular Visual-Inertial Odometry and Depth Estimation. (2019). arXiv:1911.09968 <http://arxiv.org/abs/1911.09968>

[3] ARM. 2020. CMSIS DSP Software Library. <http://www.keil.com/pack/doc/CMSIS/DSP/html/index.html>

[4] Martin Brossard, Axel Barrau, and Silvere Bonnabel. 2019. RINS-W: Robust Inertial Navigation System on Wheels. *IEEE International Conference on Intelligent Robots and Systems* (2019). <https://doi.org/10.1109/IROS40897.2019.8968593> arXiv:1903.02210

[5] Changhao Chen, Xiaoxuan Lu, Andrew Markham, and Niki Trigoni. 2018. IoNet: Learning to cure the curse of drift in inertial odometry. *32nd AAAI Conference on Artificial Intelligence, AAAI 2018* (2018). arXiv:1802.02209

[6] Changhao Chen, Xiaoxuan Lu, Johan Wahlstrom, Andrew Markham, and Niki Trigoni. 2019. Deep neural network based inertial odometry using low-cost inertial measurement units. *IEEE Transactions on Mobile Computing* (2019).

[7] Changhao Chen, Stefano Rosa, Yishu Miao, Chris Lu, Wei Wu, Andrew Markham, and Niki Trigoni. 2019. Selective Sensor Fusion for Neural Visual-Inertial Odometry. 10534–10543. <https://doi.org/10.1109/CVPR.2019.01079>

[8] Changhao Chen, P. Zhao, Chris Xiaoxuan Lu, W. Wang, A. Markham, and A. Trigoni. 2018. OxIOD: The Dataset for Deep Inertial Odometry. *ArXiv abs/1809.07491* (2018).

[9] Changhao Chen, Peijun Zhao, Chris Xiaoxuan Lu, Wei Wang, Andrew Markham, and Niki Trigoni. 2020. Deep-Learning-Based Pedestrian Inertial Navigation: Methods, Data Set, and On-Device Inference. *IEEE Internet of Things Journal* 7, 5 (2020), 4431–4441. <https://doi.org/10.1109/JIOT.2020.2966773> arXiv:2001.04061

[10] Hamed Damirchi, Rooholla Khorrambakht, and Hamid Taghirad. 2020. ARC-Net: Activity Recognition Through Capsules. *arXiv preprint arXiv:2007.03063* (2020).

[11] Frank Dellaert. 2021. Factor graphs: Exploiting structure in robotics. *Annual Review of Control, Robotics, and Autonomous Systems* 4 (2021), 141–166.

[12] Christian Forster, Luca Carlone, Frank Dellaert, and Davide Scaramuzza. 2017. On-Manifold Preintegration for Real-Time Visual-Inertial Odometry. *IEEE Transactions on Robotics* 33, 1 (2017). <https://doi.org/10.1109/TRO.2016.2597321>

[13] Andreas Geiger, Philip Lenz, and Raquel Urtasun. 2012. Are we ready for Autonomous Driving? The KITTI Vision Benchmark Suite. In *Conference on Computer Vision and Pattern Recognition (CVPR)*.

[14] Guoquan Huang. 2019. Visual-inertial navigation: A concise review. *Proceedings - IEEE International Conference on Robotics and Automation* 2019-May (2019). <https://doi.org/10.1109/ICRA.2019.8793604> arXiv:1906.02650

[15] V. Peretroukhin and J. Kelly. 2018. DPC-Net: Deep Pose Correction for Visual Localization. *IEEE Robotics and Automation Letters* 3, 3 (2018), 2424–2431. <https://doi.org/10.1109/LRA.2017.2778765>

[16] Timothy Sandy, Lukas Stadelmann, Simon Kerscher, and Jonas Buchli. 2019. ConFusion: Sensor Fusion for Complex Robotic Systems using Nonlinear Optimization. *IEEE Robotics and Automation Letters* PP, c (2019). <https://doi.org/10.1109/LRA.2019.2894168> arXiv:1806.07115

[17] Muhamad Risqi U. Saputra, Niki Trigoni, Pedro P.B. De Gusmão, Chris Xiaoxuan Lu, Yasin Almalioglu, Stefano Rosa, Changhao Chen, Johan Wahlstrom, Wei Wang, and Andrew Markham. 2020. DeepTIO: A deep thermal-inertial odometry with visual hallucination. *IEEE Robotics and Automation Letters* 5, 2 (2020). <https://doi.org/10.1109/LRA.2020.2969170> arXiv:1909.07231

[18] Brandon Wagstaff, Valentin Peretroukhin, and Jonathan Kelly. 2020. Robust Data-Driven Zero-Velocity Detection for Foot-Mounted Inertial Navigation. *IEEE Sensors Journal* 20, 2 (2020). <https://doi.org/10.1109/JSEN.2019.2944412> arXiv:1910.00529